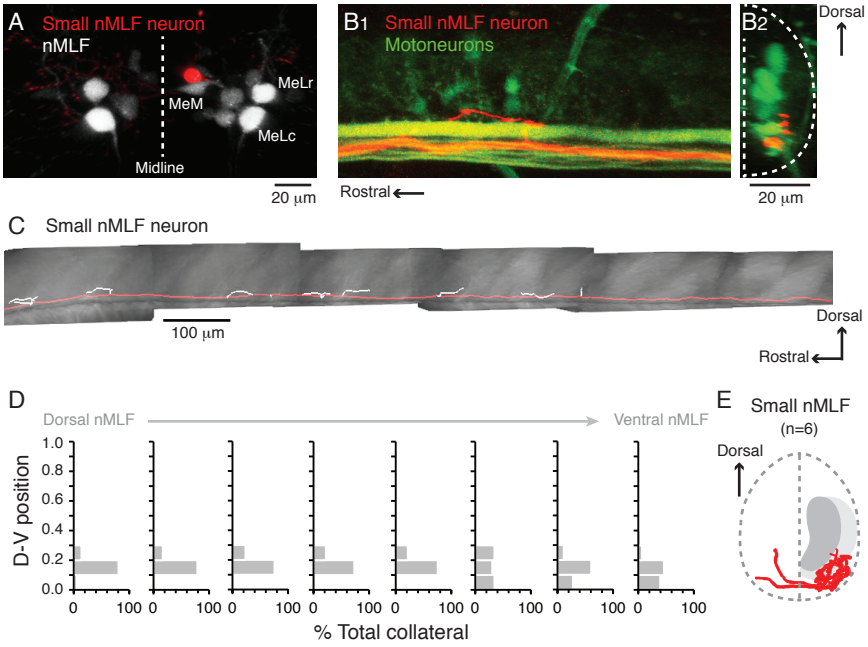

Supplemental Figure 1, Related to Figure 1 and 2. Axon Collaterals of Non-identified nMLF Neurons are Distributed Ventro-Laterally in the Spinal Cord

(A) A small, non-identified nMLF neuron labeled by single cell electroporation. This neuron is located ventrally in the nMLF, just rostral to the MeM neuron. The dashed line marks the midline of the brain.

(B) Lateral (*B1*) and cross-sectional (*B2*) views of spinal axon collaterals of the small, ventral nMLF neuron in *A*. The lateral view is a projection image from stacks lateral to the motoneuron cell body layer (~10 μm thick), while the cross-sectional view represents a collapsed image from a body segment (~80-90 μm). The dashed line marks the boundary and midline of the spinal cord.

(C) Lateral view of the reconstructed main axon (red) and collaterals (white) from body segments 5-18 of the small, ventral nMLF neuron in *A*.

(D) Percentage of collateral length at each spinal dorso-ventral division to total collateral length from eight smaller, non-identified nMLF neurons. The neurons are arranged from left to right according to their relative dorso-ventral locations in the nMLF. Analyzed axon collaterals are from various numbers of body segments (5-10~15 segments) depending on the quality of the neuronal filling. Note: values in the most ventral spinal cord division (0-0.1) in the 3 ventrally located nMLF neurons represent axon collaterals that cross the midline of the spinal cord (2 of these cells are shown in *E*).

(E) Cross-sectional view of registered reconstructed axon collaterals from 6 small nMLF neurons. These collaterals predominantly stay ventro-laterally in the neuropil layer.

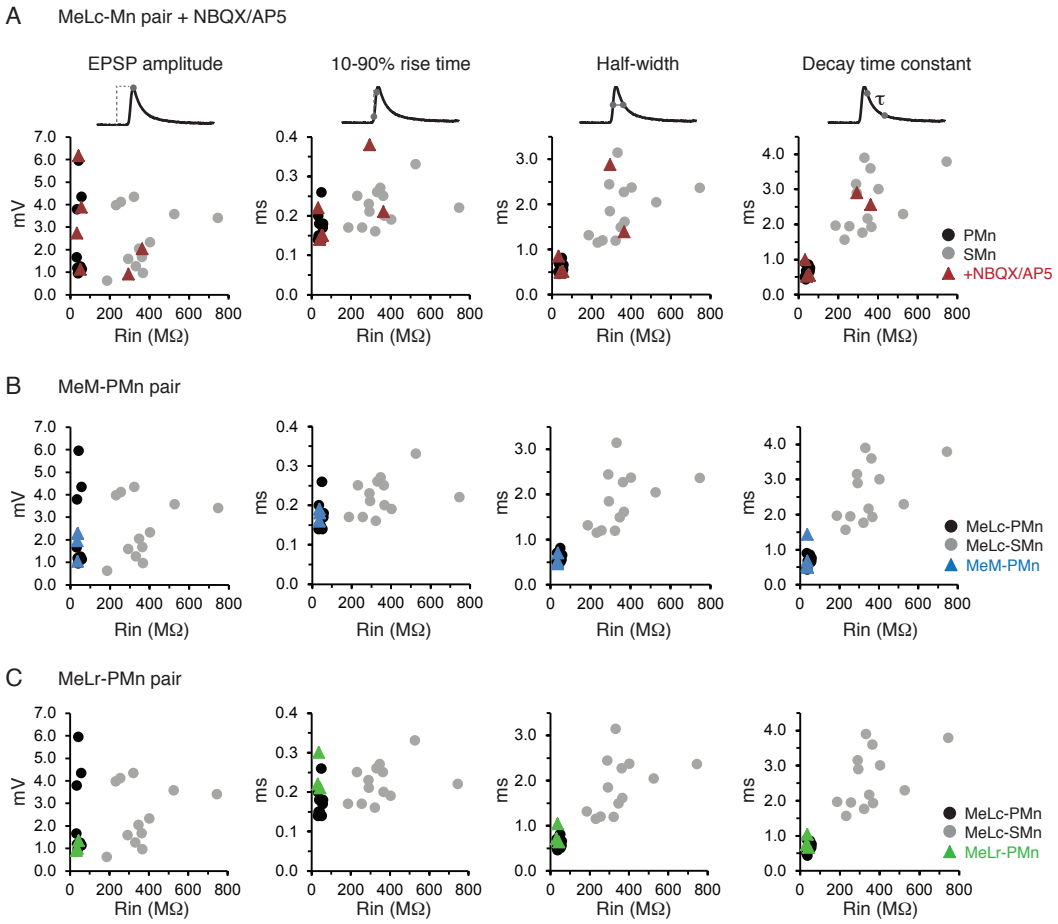

Supplemental Figure 2, Related to Figure 3. Waveform of EPSPs Elicited by Identified nMLF Neurons

(A) Properties of MeLc-elicited EPSPs versus input resistance (Rin) for primary (PMns) and secondary (SMns) motoneurons. Filled circles represent EPSPs with purely early components in control extracellular solution (black circles: PMns; gray circles: SMns). Red triangles are EPSPs in PMns (n = 4) and SMns (n = 2) in the presence of glutamate receptor antagonists (NBQX/AP5), which eliminates the possible contribution of the later chemical component to the EPSP waveform. Note that the data overlap measurements in the absence of NBQX/AP5.

(B) Blue triangles denote MeM-elicited EPSPs which contain only the early component in PMns (n = 4 pairs). Compared to MeLc-elicited EPSPs in motoneurons with various Rin (filled circles), waveform properties of MeM-elicited EPSPs in PMns are similar to those of MeLc-elicited EPSPs in PMns.

(C) Green triangles denote MeLr-elicited EPSPs which contain only the early component in PMns (n = 3 pairs). As in *B*, for PMns, the MeLr-elicited EPSPs are similar to those of MeLc-elicited EPSPs.

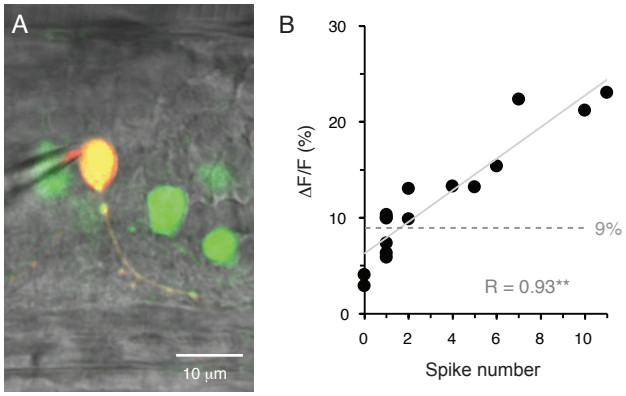

Supplemental Figure 3, Related to Figure 5. Calcium Signals Increases Linearly with the Number of Action Potentials

(A) Spinal motoneurons were retrogradely labeled with calcium-sensitive dye (green). Cell-attached recording was performed on one of the labeled motoneurons in conjunction with monitoring calcium transients during tail stimulation. The recorded cell was broken into at the end of the recording and dialyzed with the red Alexa Fluor 568 contained in the patch solution to confirm the extracellular recording was truly from this cell (yellow).

(B) There is positive correlation between calcium signal change (ΔF/F) and the number of action potentials. Trend line is a linear fit. **: $p<0.05$ following Pearson linear correlation test (R). A 9% ΔF/F threshold line is marked on the graph. The averaged ΔF/F of calcium signal change when the cell fires one action potential is close to the 9% threshold we used for our response reliability analysis (mean, 8.30 ± 2.02%).

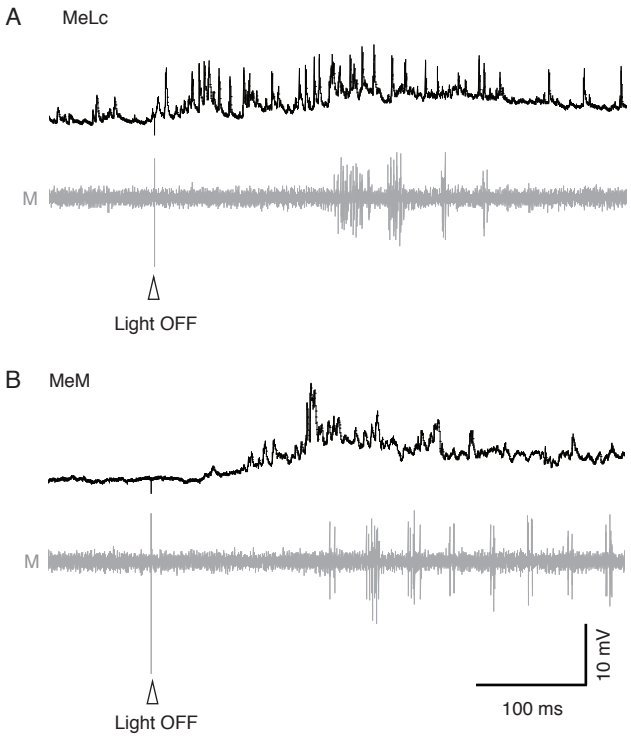

Supplemental Figure 4, Related to Figure 6. Light Evoked Synaptic Drive in MeLc and MeM Neurons Precedes Swimming Activity

(A-B) Example traces of whole-cell recordings from the MeLc (*A*) and MeM (*B*) and peripheral motor nerve activity (M) in response to light offset (at open arrowheads).

Supplemental Experimental Procedures

Fish

Wild-type, *mitfa-/-* (nacre; Lister et al., 1999), and *parg*^{mn2Et} (Balciunas et al., 2004) zebrafish larvae (*Danio rerio*) were obtained from an in-house facility (Aquatic Habitats, Beverly, MA). Nacre mutants were used for brain imaging and electrophysiological experiments, due to their lack of pigment and the resulting ease of visualization. The *parg*^{mn2Et} enhancer trap line enabled the identification of putative connections to spinal motoneuron labeled with GFP. All zebrafish were maintained at 28.5°C in system water (pH = 7.3; conductivity = 550 μS), but experiments were performed at room temperature (~22°C) using zebrafish larvae between 4 to 6 days post fertilization (dpf) when they are free-swimming. At this stage, zebrafish have not yet sexually differentiated and are still nourished by their yolk. All procedures described below conform to NIH guidelines regarding animal experimentation and were approved by Northwestern University Institutional Animal Care and Use Committee.

Electrophysiological Recordings and Analysis

Electrophysiology experiments were performed as described previously (Bhatt et al., 2007; Masino and Fetcho, 2005). Briefly, zebrafish larvae were immobilized by immersion in extracellular solution containing the neuromuscular blocker, α-bungarotoxin (0.1% w/v; composition in mmol/L: 134 NaCl, 2.9 KCl, 1.2 $MgCl_2$, 2.1 $CaCl_2$, 10 HEPES, 10 glucose, adjusted to pH 7.8 with NaOH; α-bungarotoxin purchased from Tocris Bioscience). After 5–10 minutes, immobilized larvae were transferred to a Sylgard lined glass-bottom dish containing extracellular solution and pinned down through the notochord using electrolytically sharpened tungsten pins. The skin from close to the caudal end of the swim bladder to 3-5 segments from the tail tip was carefully removed from one side using fine forceps to provide access to the motor nerves. For spinal motoneuron recordings, the muscle overlying the 1-2 spinal segments was carefully removed using a dissecting pin. For nMLF recordings, the head was rotated dorsal-side up and secured by placing two tungsten pins behind the eyes, and a small patch of skin at the rostral edge of the left tectum was removed to allow an easier entry to the brain for the recording pipette. The preparation was then transferred to the physiological recording apparatus, comprised of an upright microscope (AxioExaminer, Zeiss) equipped with a 40x/1.0 NA water immersion objective, and two motorized micromanipulators (MPC-200/ROE-200; Sutter Instruments).

For whole-cell recordings, standard wall glass capillaries were pulled to make recording pipettes with resistances between 10–16 MΩ. The recording pipette was backfilled with patch solution (composition in mmol/L: 125 K-gluconate, 4 $MgCl_2$, 10 EGTA, 10 HEPES, 4 Na_2ATP, adjusted to pH 7.3 with KOH), and positive pressure was maintained using a pneumatic transducer (DPM-1B; Fluke Biomedical) while the pipette was carefully advanced into either the brain (10-15 mmHg) or the spinal cord (20-40 mmHg). Once the pipette tip was in contact with the soma of the targeted cell, the pressure was reduced to atmosphere. A small amount of oral suction was delivered to achieve the GΩ seal. When the pipette was cell-attached, a holding current was applied to maintain the cell at –65 mV and brief oral suction pulses were delivered to rupture the seal. Alexa Fluor 568 was included in the patch solution (final concentration 50 μmol/L) to visualize cell morphology at the end of experiments using a cooled CCD camera (Rolera-XR, Q-Imaging). Images were captured using Qcapture Suite imaging software (Q-Imaging).

For patch recordings of identified nMLF neurons, descending neurons were first retrogradely labeled with 10% w/v fluorescein (3000MW, Invitrogen) in patch solution injected to the spinal cord at around segment 20 the day before experimentation. Cell-attached recordings were performed for some nMLF neurons during the GΩ seal to monitor firing pattern without interfering with the internal composition of the neuron. The firing pattern was similar for cell-attached and

whole-cell recordings so data from the two recording modes were pooled for analysis. For paired recordings, spinal motoneurons were targeted first as described above, followed by neurons in the nMLF. To test for monosynaptic connections, the solution was substituted with high divalent ion extracellular solution (composition in mmol/L: 119.1 NaCl, 2.9 KCl, 4.8 $MgCl_2$, 8.4 $CaCl_2$, 10 HEPES, 10 glucose, adjusted to pH 7.8 with NaOH) delivered by a gravity-fed perfusion system. For pharmacological experiments, the glutamate receptor antagonists NBQX and D-AP5 were dissolved in extracellular solution and added to the perfusate (10 μmol/L and 100 μmol/L final concentration, respectively).

For peripheral motor nerve recordings, pipettes were fashioned from the same ones used for whole-cell recording, however the tip was cut to make a 20-50 μm opening. A microforge (MF-830; Narishige) was used to simultaneously heat polish and bend the tip to compensate for the approach angle (~20°), which improved the contact between the electrode and the muscle. The pipette was then filled with extracellular solution and placed on the muscle cleft. To evoke motor activity, a visual stimulus was provided by a blue light emitting diode (LED, RadioShack, peak emission wavelength: 468nm). Blue light was chosen because the dichroic mirror on the confocal microscope used for calcium imaging effectively filters this wavelength out (for more details, see *In Vivo Calcium Imaging* below). The LED was placed 1.5 cm from the fish, and was triggered by an isolated stimulator (model 2100; A-M Systems; 2.5-3.6 V; duration: 2-10 sec). Turning on/off the LED light generated a 10-140 lux increase or decrease of ambient illumination, as assessed using a light meter (model 401025; Extech Instruments). The location of the LED was adjusted using a manual micromanipulator (YOU-3; Narishige).

Whole-cell recordings were acquired using a Multiclamp 700B amplifier, a Digidata series 1440A digitizer, and pClamp software (Molecular Devices). Standard corrections for bridge balance and electrode capacitance were applied in current-clamp mode. Electrical signals were filtered at 30 kHz and digitized at 100 kHz at a gain of 10 (feedback resistor, 500 MΩ). Extracellular signals from peripheral motor nerve activity were recorded in current clamp mode, at a gain of 500 with low and high frequency cutoffs set at 300 and 4000 Hz, respectively. All electrophysiological data were analyzed using DataView (Heitler, 2009) and custom written MATLAB scripts. Only cells with stable resting membrane potential below –50mV and overshooting action potentials were included in the analysis. A calculated liquid junction potential of –16 mV has not been corrected for our recordings.

Putative connections between nMLF neurons and spinal motoneurons were tested using 500 ms duration depolarizing current steps. For analysis, EPSPs were aligned to the peak of presynaptic nMLF action potential. The averaged motoneuron membrane potential 1 ms before the nMLF action potential was used as the baseline and was subtracted from each EPSP trace. EPSP latency was defined as the time interval between the peak of the presynaptic nMLF action potential and the peak of the postsynaptic early electrical or later chemical components. EPSP decay time constants were calculated by a single exponential fit between 20-80% of the peak amplitude. For all measures, between 10-100 EPSPs from each motoneuron were used. The reliability of the chemical component for each motoneuron was calculated as the number of EPSPs with clear chemical components divided by the total number of MeLc action potentials. To avoid the potential confounding effect of chemical synapse fatigue, we examined reliability when the MeLc was firing at relatively low rates (<100 Hz).

To assess the membrane time constant of spinal motoneurons, square hyperpolarizing current pulses (1ms; 100 Hz; –10 to –500 pA, depending on the input resistance of the motoneuron, to achieve a ~4 mV deflection in all cells) were injected into the motoneuron in whole-cell, current clamp recording mode. Voltage responses from 100 pulses were averaged, and the decay phase of the averaged voltage response trace from 0-8 ms after the end of current pulse was fit with

single exponential to get the membrane time constant. Input resistance was measured from voltage changes in response to 5-10, 500 ms hyperpolarizing current steps using V=IR.

For motor nerve recordings, response latency to light ON/OFF was defined as the interval between the stimulus and the onset of the first swim burst. Duty cycle represents the ratio of a swim burst occupying a single cycle of swimming and is calculated as burst duration divided by time interval between the onset of successive motor bursts (cycle period). Bilateral motor nerve activity was recorded and analyzed when comparing the duty cycle between spontaneous and light elicited swimming. For spike phase analysis, the rostral-caudal delay of motor nerve bursts was corrected by 1ms/body segment (Kimura et al., 2013; McLean et al., 2008). To examine firing rhythmicity of spinal motoneurons and nMLF neurons, individual swim cycles were binned into ten equal time windows, and the ratio of action potentials occurred within each bin was analyzed. Swim bouts used for this analysis were elicited by light onset and offset.

In Vivo Calcium Imaging and Analysis

In vivo calcium imaging was performed as described previously (McLean et al., 2007). Briefly, 10% w/v calcium green dextran (3,000 MW, Invitrogen) in patch solution was used as a calcium indicator. To label spinal motoneurons, calcium green was pressure injected into one or two segments of ventral musculature close to the mid-body of anesthetized larval zebrafish using a microinjector (Model IM300, Narishige). To label nMLF neurons, calcium green was pressure injected into the spinal cord around muscle segment 20. Fish were placed in a 28 °C incubator overnight to ensure the neurons were retrogradely labeled.

Image acquisition was performed in conjunction with peripheral motor nerve recordings, as described above. The head was oriented and stabilized dorsal-side up with two tungsten pins behind the eyes. This preparation allowed us to image nMLF neurons from the top or spinal motoneurons from the side (Figure 5A). In 5 of 11 fish, motoneuron imaging was performed without orienting the head dorsal-side up. The recruitment pattern of spinal motoneurons in response to light was similar regardless of head orientation, so these data were pooled together for analysis. Images were acquired using a 488 nm wavelength laser on a confocal microscope (Zeiss LSM 710) with a Zeiss 40x/1.0 NA water immersion objective and Zen imaging software. The scanning frame rate was between 100-250 ms/frame. A TTL signal was sent out from the imaging software to synchronize calcium imaging, motor nerve recordings, and sensory stimuli. A high-resolution Z-stack of the somata of recorded neurons was always taken at the end of the experiment to assess the location of motoneurons in the spinal cord, and nMLF neurons in the midbrain. For 3D image registration, high-resolution Z-stacks from multiple fish were aligned using a custom MATLAB script (Koyama et al., 2011) that was interfaced with the neuronal reconstruction software, Imaris (Bitplane). The quality of registration was confirmed by the proper alignment of primary motoneurons for spinal cord, and the MeL neurons for the nMLF. Cell body surfaces were reconstructed in Imaris for imaged neurons and color-coded according to their response reliability to light (see below).

To analyze activity changes of neurons in response to light, regions of interest (ROIs) were created around the cell body, and the fluorescence of each ROI at each time frame was measured using ImageJ. The averaged fluorescence one second before the stimulus was used as the baseline fluorescence (F_0), and the change of the fluorescence ($\Delta F/F = [F-F_0]/F_0$) was calculated using a custom MATLAB script. We only analyzed trials where the fish showed motor nerve activity in response to the LED stimulus to ensure that calcium transients were associated with motor output. A 9% $\Delta F/F$ increase was used as the threshold for neuronal activation (Figure S1; see also, Bhatt et al., 2007; Fetcho and O'Malley, 1995). To calculate the dorso-ventral location of motoneuron somata, the center of the somata was normalized to the dorsal (1) and ventral (0) edges of the spinal cord. For the relative medio-lateral (M-L) location of nMLF neurons

in the midbrain, the center of the somata was normalized to the midline of the brain (0) and the center of the MeLr neuron cell body (1). Measurements of peak amplitudes during light stimuli represent the maximum calcium signal associated with the first swim bout after the stimulus. Response reliability was calculated as the number of trials when the neurons showed > 9% ΔF/F divided by the number of total trials and expressed as a percentage. Each cell had to receive at least three stimulation trials (light onset and offset) to be included in the analysis.

Single-Cell Electroporation

Single cell electroporation was performed as described previously (Bhatt et al., 2004). Briefly, nMLF neurons were first retrogradely labeled with 10% w/v fluorescein (in both wild-type and *nacre* larvae) or tetramethylrhodamine 3,000 MW dextran (for *parg*^{mn2Et} larvae) in patch solution and allowed to recover overnight. Larval zebrafish were then anesthetized and embedded dorsal side up in 1.4 % w/v low melting agar in a glass bottomed dish. A drop of MS-222 solution was used to cover the agar to keep the fish anesthetized through the labeling process, which was performed on the confocal microscope. A glass pipette identical to ones used for whole-cell recording was filled with 10% w/v Alexa Fluor 647 (10,000 MW, Invitrogen) in patch solution, and was advanced down to the nMLF using a motorized micromanipulator (MPC-200/ROE-200) until it directly contacted the target neuron. A train of current pulses (2-4 V; pulse duration: 1 ms; pulse interval: 2 ms; total length: 0.5 s) was then applied via an isolated stimulator. When performing dual labeling of two identified nMLF cells in the same fish, fluorescein was used to retrogradely label nMLF neurons for targeting, and neurons were subsequently electroporated with either tetramethylrhodamine or Alexa Fluor 647. A high-resolution Z-stack of the nMLF was taken right after electroporation because the cell body and dendrites filled immediately. The fish was then removed from the agar and left to recover in system water for one hour to allow the dye to fill the axon collaterals.

To image axon collaterals in the spinal cord, the fish was immobilized with α-bungarotoxin and embedded on their side in agar. Multiple Z-stacks were taken from the hindbrain-spinal cord boundary to the dye injection site, and these Z-stacks were then stitched together with XuvTools into a single image (Emmenlauer et al., 2009). Imaris was used to reconstruct axon collaterals, and a custom MATLAB program was then used to analyze the length of the reconstructed axon collaterals at each normalized dorso-ventral (D-V) division (Kishore and Fetcho, 2013). The relative contribution of collaterals from the MeLr, MeLc, and MeM neurons at each D-V division (Figure 1I) was calculated as the average length of total collaterals within body segments 5-14 of each cell type divided by the sum of the averaged collateral length from all three cell types. To align the medio-lateral distribution of axon collaterals of nMLF neurons from multiple fish, a snapshot of the cross-sectional view of a single spinal cord segment (~80-90 μm) between myotomes 7-9 was created in Imaris. The most dorsal and ventral edges of spinal cord, the Mauthner axons, and the GFP-positive motor column in the *parg*^{mn2Et} larvae were used as references for the registration.

Statistical Analysis

Before statistical analysis, all data were tested for normality to determine whether parametric versus nonparametric examinations were appropriate. Consequently, comparisons of the means between two independent groups were performed using a Student's t-test or a Mann-Whitney U-test, comparisons of the variances between three groups were performed using Mann-Whitney U-tests followed by Bonferroni correction, the comparison of two cumulative distributions was performed using Kolmogorov-Smirnov Test, and correlations were determined using a Pearson linear correlation test or a Spearman rank R correlation test. Analysis was performed using StatPlus and Microsoft Excel. Data are reported as means plus or minus standard errors unless noted otherwise.

Supplemental References

Balciunas, D., Davidson, A.E., Sivasubbu, S., Hermanson, S.B., Welle, Z., and Ekker, S.C. (2004). Enhancer trapping in zebrafish using the Sleeping Beauty transposon. BMC Genomics 5, 62.
Bhatt, D.H., McLean, D.L., Hale, M.E., and Fetcho, J.R. (2007). Grading movement strength by changes in firing intensity versus recruitment of spinal interneurons. Neuron 53, 91-102.
Bhatt, D.H., Otto, S.J., Depoister, B., and Fetcho, J.R. (2004). Cyclic AMP-induced repair of zebrafish spinal circuits. Science 305, 254-258.
Emmenlauer, M., Ronneberger, O., Ponti, A., Schwarb, P., Griffa, A., Filippi, A., Nitschke, R., Driever, W., and Burkhardt, H. (2009). XuvTools: free, fast and reliable stitching of large 3D datasets. J Microsc 233, 42-60.
Fetcho, J.R., and O'Malley, D.M. (1995). Visualization of active neural circuitry in the spinal cord of intact zebrafish. J Neurophysiol 73, 399-406.
Heitler, W.J. (2009). Practical tools for analysing rhythmic neural activity. J Neurosci Methods 185, 151-164.
Kimura, Y., Satou, C., Fujioka, S., Shoji, W., Umeda, K., Ishizuka, T., Yawo, H., and Higashijima, S.I. (2013). Hindbrain V2a neurons in the excitation of spinal locomotor circuits during zebrafish swimming. Curr Biol 23, 843-849.
Kishore, S., and Fetcho, J.R. (2013). Homeostatic regulation of dendritic dynamics in a motor map in vivo. Nat Commun 4, 2086.
Koyama, M., Kinkhabwala, A., Satou, C., Higashijima, S., and Fetcho, J. (2011). Mapping a sensory-motor network onto a structural and functional ground plan in the hindbrain. Proc Natl Acad Sci U S A 108, 1170-1175.
Lister, J.A., Robertson, C.P., Lepage, T., Johnson, S.L., and Raible, D.W. (1999). nacre encodes a zebrafish microphthalmia-related protein that regulates neural-crest-derived pigment cell fate. Development 126, 3757-3767.
Masino, M.A., and Fetcho, J.R. (2005). Fictive swimming motor patterns in wild type and mutant larval zebrafish. J Neurophysiol 93, 3177-3188.
McLean, D.L., Fan, J., Higashijima, S., Hale, M.E., and Fetcho, J.R. (2007). A topographic map of recruitment in spinal cord. Nature 446, 71-75.
McLean, D.L., Masino, M.A., Koh, I.Y., Lindquist, W.B., and Fetcho, J.R. (2008). Continuous shifts in the active set of spinal interneurons during changes in locomotor speed. Nat Neurosci 11, 1419-1429.